Shigematsu *et al.*
Progress in Earth and Planetary Science (2022) 9:34
https://doi.org/10.1186/s40645-022-00492-5

Progress in Earth and Planetary Science

METHODOLOGY

Open Access

Fabrication of dense albite aggregates by hot pressing

Norio Shigematsu[1*], You Zhou[2], Hideki Hyuga[2], Yu-ichi Yoshizawa[2] and Masanori Kido[1,3]

Abstract

Synthetic rocks are used in laboratories to measure the physical and chemical properties of Earth's constituent minerals in order to understand Earth's interior. To understand the phenomena in the middle and upper crust, dense aggregates of Na-rich plagioclase are necessary. Therefore, we explored a method of fabricating dense aggregates of albite with low porosities, homogeneous microstructures, the absence of melt and sample sizes larger than a cubic centimetre using hot pressing by solid-state sintering. We conducted multiple experiments in which we varied the particle sizes, the agglomerations of powder, the method of forming, the sintering temperature, and the pressure and duration of the hot pressing. Two particle size fractions of powder, less than two micrometres and less than a few hundred nanometres, were prepared by pulverisation and decantation of natural albite powder. Because fine-grained albite powder seems to agglomerate easily, a technique to dry and disperse the powder was also developed. Hot pressing was carried out at temperatures of 1000–1150 °C and pressures of 40–120 MPa. The following were found to be important in obtaining dense aggregates of albite: (1) powders with a particle size less than a few hundred nanometres; (2) powders are adequately dispersed; and (3) preparation of green bodies by slip casting, which makes hot pressing efficient. A dense albite aggregate can then be fabricated using hot pressing at a temperature of 1080 °C and pressure of 100 MPa by solid-state sintering.

Keywords: Albite, Hot pressing, Solid-state sintering, Fine powders, Slip casting

1 Introduction

The physical and chemical properties of Earth's constituent minerals have often been measured in laboratories with the aim of understanding Earth's interior, and synthetic rocks have typically been used for this purpose (e.g. Karato 2010; Koizumi et al. 2010; Luan and Paterson 1992). Recently, synthetic polycrystalline aggregates of rock-forming minerals have been produced by sintering fine-grained powders, and the experiments using these synthetic rocks have improved our understanding of the rheology of Earth's mantle and lower crust (e.g. Hiraga et al. 2010; Miyazaki et al. 2013; Tsubokawa and Ishikawa 2017; Yabe et al. 2020).

Feldspar is the main constituent mineral of Earth's crust, and synthesised feldspar aggregates have been used in experiments to measure their physical and chemical properties (e.g. Carpenter 1991; Farver and Yund 1995a, b; Rybacki and Dresen 2000; Tullis and Yund 1985). Na-rich plagioclase is particularly common in the middle and upper crust, and the investigation of the physical and chemical properties of polycrystalline albite is therefore important if we wish to understand the behaviour of the middle and upper crust. For this purpose, it is necessary to develop methods of sintering albite.

Two main methods have been used in previous studies to synthesise dense aggregates of feldspar. One is the annealing of glass with the composition of feldspar, which allows fine grains of feldspar to crystallise from the glass (e.g. Carpenter 1991; Dresen et al. 1996; Farver

*Correspondence: n.shigematsu@aist.go.jp

[1] Research Institute of Earthquake and Volcano Geology, Geological Survey of Japan, National Institute of Advanced Industrial Science and Technology, Tsukuba 305-8567, Japan
Full list of author information is available at the end of the article

and Yund 1995a; Fukuda et al. 2018; Rybacki and Dresen 2000; Rybacki et al. 2010). The other is hot pressing of a crystalline powder with a particle size of less than a few micrometres (e.g. Farver and Yund 1995b; Tullis and Yund 1985).

One of the problems with feldspar aggregates prepared by the annealing of glass is the presence of the residual glass at the grain junctions (Rybacki and Dresen 2000; Rybacki et al. 2010). A Griggs-type deformation apparatus or piston cylinder has previously been used for the hot pressing of a crystalline powder of feldspar that resulted in samples with a very limited size (normally less than a cubic centimetre). Another issue with synthesising dense albite aggregates is that the melting temperature of albite is as low as 1100 °C (Deer et al. 1992); this makes it more difficult to sinter albite than other minerals such as olivine or pyroxene (e.g. Hiraga et al. 2010; Koizumi et al. 2010; Miyazaki et al. 2013; Tasaka and Hiraga 2013; Tsubokawa and Ishikawa 2017). Several studies previously synthesised dense albite aggregate using a Griggs-type deformation apparatus or piston cylinder by hot pressing (e.g. Tullis and Yund 1985; Farver and Yund 1995a), although the sample sizes were small. We further explored a method of fabricating dense aggregates of albite with low porosities, homogeneous microstructures, the absence of melt and sample sizes larger than a cubic centimetre using an industrial hot pressing furnace by solid-state sintering at the pressures as low as possible.

2 Experimental procedures

Several process parameters have a strong influence on the results of sintering, and they involve the particle size of the powder, the dispersion of the powder, the method of forming, the sintering temperature, and the pressure and duration of the hot pressing. Therefore, we examined various combinations of these process parameters. After the hot pressing, we evaluated the results and determined the best combination of process parameters.

In general, the particle size of the powder has a strong effect on shrinkage behaviour during sintering, and the smaller the particle size, the faster the shrinkage (e.g. Kang 2005). For our study, we used industrial albite powders (FN-100 Kyoritsu material, Nagoya, Japan) that were milled from natural albite, and we then pulverised the powders further for 25 s using a HERZOG HP-MS60 automatic pulveriser at the GSJ Laboratory (GSJ-Lab) of the Geological Survey of Japan, National Institute of Advanced Industrial Science and Technology (GSJ, AIST). This automatic pulveriser is a vibration disc mill with an automatic cleaning system to reduce cross-contamination. We found that pulverisation of < 30 s is necessary to avoid significant contamination by tungsten carbide. However, we did detect some contamination due to the pulverisation, which is described later. X-ray diffraction (XRD) analyses were performed using a RIGAKU RINT 2500 X-ray diffractometer (Cu $K\alpha_1$) at the GSJ-Lab of the GSJ, AIST, to reveal the mineral phases of the raw powders. Fractions that were finer than the desired particle size were separated by decantation. The powders were dispersed in water, and the suspension left to stand. The particle size was adjusted by changing the duration of decantation and separating the top layer of the suspension, leaving a 2-cm-deep suspension. We adopted two durations of decantation, 6 and 24 h, at a temperature of 20 °C. After these decantations, denser fine powder fractions were obtained using a centrifuge. The particle size of the fine-grained fractions was evaluated using a HITACHI SU-3500 scanning electron microscope (SEM) installed at the GSJ-Lab of the GSJ, AIST. We refer to the powders after these two durations of decantation as "powders after 6 h of decantation" and "powders after 24 h of decantation", respectively.

Agglomeration of powders often causes the formation of secondary particles, and this sometimes results in heterogeneous sintering. Because fine albite powders appear to agglomerate easily, a technique to dry and adequately disperse the powders is necessary. In some of our experiments, the suspension after the decantation was simply frozen at − 40 °C, and water (ice) was sublimated (freeze-dried) using a Latent Life Science LFD-1000DS freeze dryer at the Research Institute of Geology and Geoinformation of the GSJ, AIST. In other experiments, we froze the suspension after decantation under alternating magnetic fields at − 40 °C, and this is known as the cell alive system (CAS), which prevents the formation of large ice crystals. By using alternating magnetic fields, the super-cooled state of water can be stably achieved, and uniform cooling results in the formation of ice crystals of minimal size (e.g. Morono et al. 2015). Before freezing, we dissolved 10 wt% ethanol in the suspension to reduce the emission of latent heat. The emission of latent heat during freezing causes a large temperature gradient within the freezing suspension (Morono et al. 2015), and a temperature gradient promotes unidirectional grain growth of the ice crystals along the temperature gradient (Fukushima et al. 2013). Dried powders were observed using a polarising optical microscope after dispersion of the powders in water. Dried powders were also observed using the HITACHI SU-3500 SEM.

Before hot pressing and after the aforementioned procedures, the powders were placed in a carbon die for hot pressing and cold-pressed at 20 MPa. In some experiments, a green body was prepared from the slurry of fine-grained powder using the technique of slip casting before cold pressing. To prepare a green body, the dried powder was sieved with a mesh size of 125 μm, and the slurry was

Table 1 Combinations of process parameters in the experiments

Exp. No.	Duration of decantation (hours)*	Freeze-drying (FD) method	Forming method	Duration of dewax (hours)	Hot pressing temperature (°C)	Hot pressing pressure (MPa)	Duration of hot pressing (hours)
#1	6	Normal FD	Cold Pressing	–	1150	50.0	6
#2	6	Normal FD	Cold Pressing	–	1125	50.0	6
#3	6	Normal FD	Cold Pressing	–	1100	50.0	1
#4	6	Normal FD	Cold Pressing	–	1000	50.0	5
#5	6	Normal FD	Cold Pressing	–	1050	50.0	19
#6	24	Normal FD	Cold Pressing	–	1100	50.0	17
#7	24	Normal FD	Cold Pressing	–	1113	50.0	17
#8	24	Normal FD	Cold Pressing	–	1100	50.0	100
#9	24	Normal FD	Cold Pressing	–	1080	100.0	1
#10	24	Normal FD	Cold Pressing	–	1080	100.0	18
#11	24	CASFD	Cold Pressing	–	1080	100.0	36
#12	24	CAS FD	Cold Pressing	–	1080	100.0	38
#13	24	CAS FD	Slip Casting	5	1080	120.0	16
#14	24	CAS FD	Cold Pressing	–	1080	80.0	16
#15	24	CAS FD	Cold Pressing	–	1080	100.0	16
#16	24	CAS FD	Slip Casting	–	1080	100.0	16
#17	24	CAS FD	Slip Casting	2	1080	100.0	16
#18	24	CAS FD	Slip Casting	26	1080	100.0	26

*Powders after 6 h decantation are smaller than 2 μm, and those after 24 h decantation are smaller than 500 nm

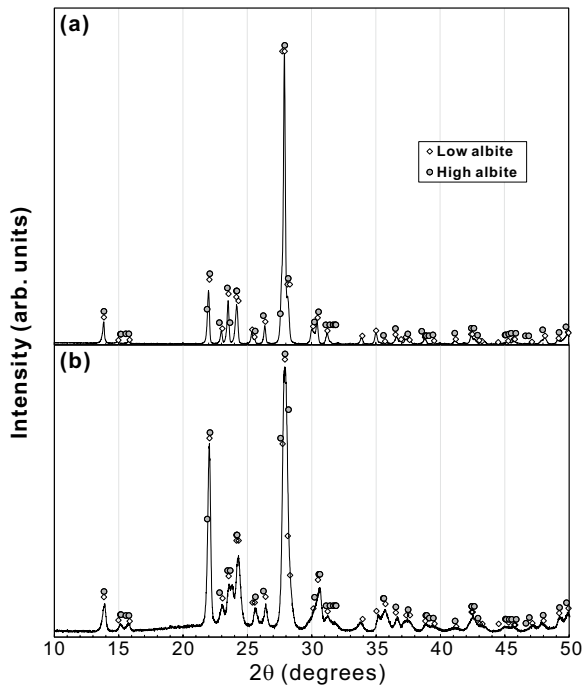

Fig. 1 Results of X-ray diffraction analyses of **a** raw powder before hot pressing, and **b** a hot-pressed sample (Exp. #12)

prepared by mixing it with pure water to which the dispersant A-6114 (Toagousei Co. Ltd., Tokyo, Japan) had been added. The concentration of the dispersant is ~ 10%. The slurry was then placed in an acrylic tube, and the water in the slurry was absorbed by a gypsum mould (Li et al. 1991). After forming a green body, the organic matter in it was combusted at 600 °C, and this procedure is called dewaxing.

The cold-pressed samples were then hot-pressed in a vacuum at temperatures of 1000–1150 °C, pressures of 50–120 MPa and for durations of 1–100 h using a Fujidempa High Multi 10,000 high-temperature furnace at AIST Chubu. The shrinkage behaviour during hot pressing was monitored with a displacement meter attached to the high-temperature furnace. Because the displacement meter was not calibrated, it was impossible to obtain an absolute value of displacement.

After hot pressing, the shapes and weights of the samples were measured after grinding the surfaces to evaluate the densification. The features of the samples were also checked visually. It is possible to estimate the apparent density by comparing the measured shape and weight with the known density of albite (2.62×10^3 kg m^{-3}; Deer et al. 1992). The volumes of some samples were also

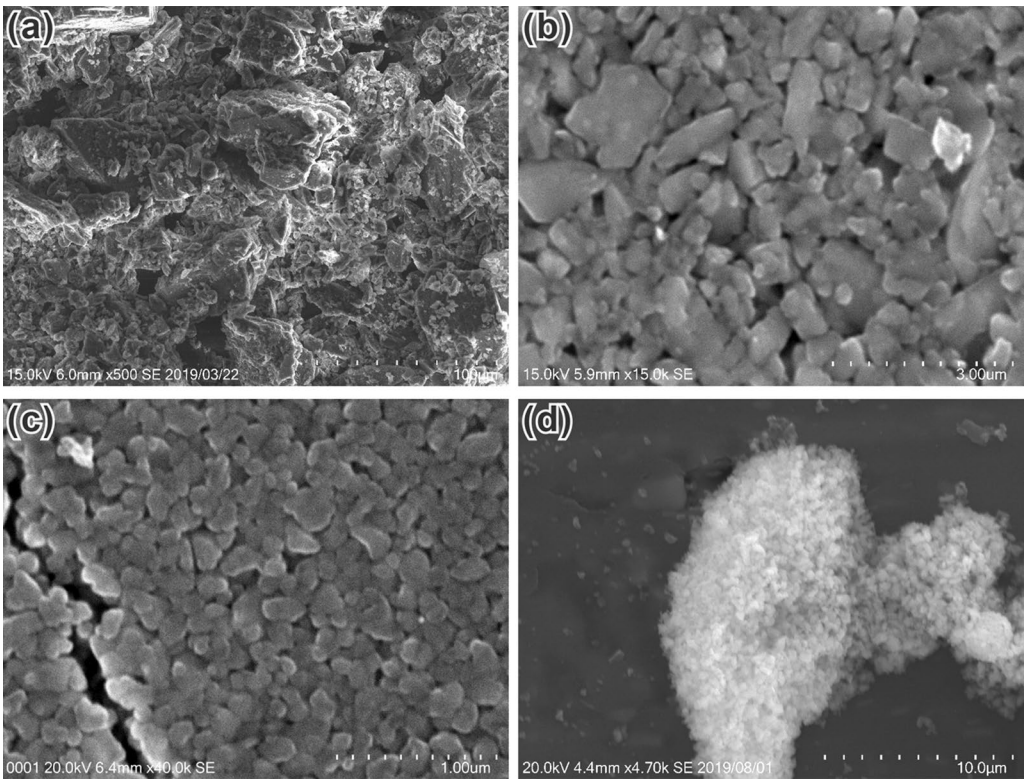

Fig. 2 SEM images of powders. **a** Raw albite powder before pulverisation. **b** Powder after pulverisation and 6 h of decantation. **c** Powder after pulverisation and 24 h of decantation. **d** Example of an agglomerated secondary particle formed after freeze-drying under CAS conditions

measured using Archimedes' principle. The samples were placed in water, and the buoyancy forces were measured at a water temperature of 20 °C. The volume can be calculated by dividing the buoyancy forces by the density of water at 20 °C (0.998×10^3 kg m^{-3}). We measured the volume three or four times and calculated the average values. The measurements obtained using Archimedes' principle are possibly unreliable for porous samples, because we did not measure the buoyancy forces after the samples had completely absorbed water. The mirror-polished surfaces of samples were observed to evaluate the results of sintering using the HITACHI SU-3500 SEM, and the chemical compositions of some samples were measured using an X-max 80 SEM–EDS (energy-dispersive spectrometer; Oxford Instruments) mounted on the HITACHI SU-3500 SEM. We also determined the chemical elements of particles that appeared to be bright in the SEM images. The chemical compositions were measured quantitatively for one sample that was densely sintered (i.e. a dense albite aggregate), as the presence of pores and the small particle size make quantitative analysis difficult. For the same sample, the mineral phases were determined using the RIGAKU RINT 2500 X-ray diffractometer. The mirror-polished surface of the dense albite aggregate was annealed for 51 h at 1050 °C in the atmosphere, and the annealed mirror-polished surface was observed with the HITACHI SU-3500 SEM. The annealing resulted in the thermal etching along grain boundaries. For another sample that was densely sintered, we also observed the grain structures with a Topcon EM-002B transmission electron microscope (TEM) installed at AIST Tsukuba West using an accelerating voltage of 120 kV. The TEM foil was prepared using a GATAN PIPS 691 ion polisher at the GSJ-Lab of the GSJ, AIST. The combinations of process parameters used in our experiments are summarised in Table 1.

3 Results and discussion

3.1 Particle sizes and mineral phases of powders before sintering

The result of an XRD analysis of raw powder before sintering is shown in Fig. 1a. Although many peaks appear because of the triclinic symmetry of plagioclase, most of the peaks can be indexed as either of low albite or high albite. The low- and high-albite crystal structures depend on temperature owing to the ordering and disordering of Al and Si atoms (Deer et al. 1992). Although both low albite and high albite can account for most of the peaks,

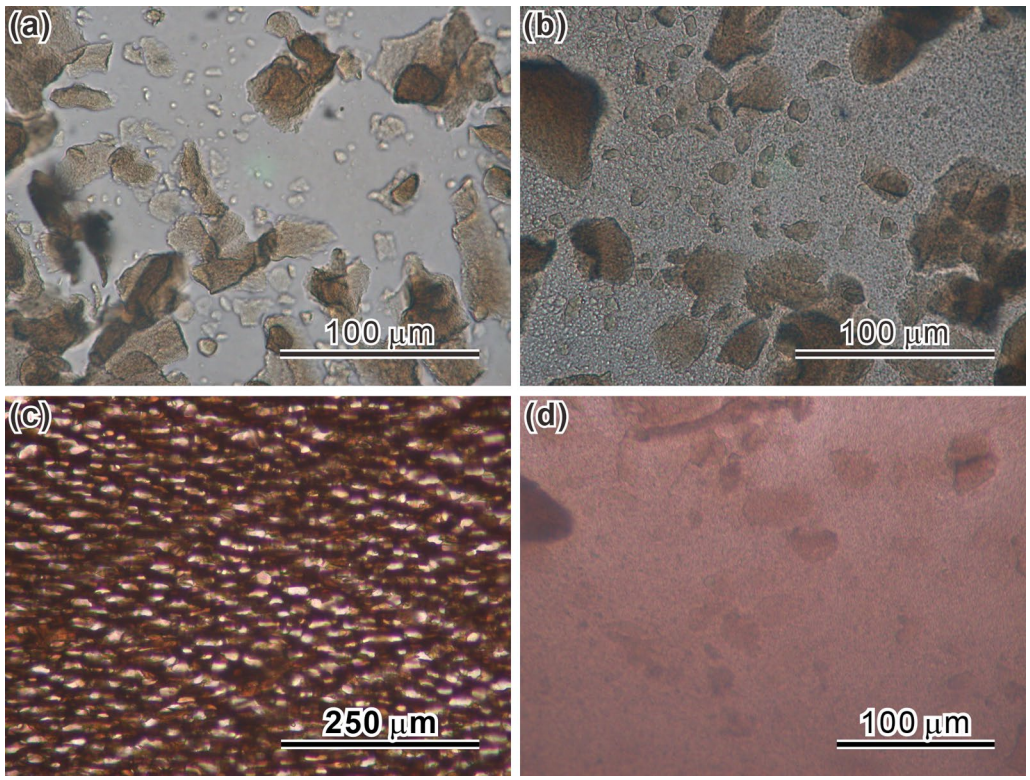

Fig. 3 Optical images of agglomerated secondary grains. **a** Freeze-dried powder without CAS conditions under plane-polarised light (PPL). **b** Freeze-dried powder with pure water solvent and CAS conditions (PPL). **c** Frozen suspension with pure water solvent under CAS conditions (PPL). **d** Freeze-dried powder with ethanol as the dissolved solvent and CAS conditions (PPL)

high albite cannot account for some peaks, such as those at 33.77° ($\bar{1}32$) and 35.18 ($24\bar{1}$), and this suggests that the raw powder consists mainly of low albite.

The sizes of particles in most of the raw albite powders before pulverisation were larger than a few micrometres, but some particles were almost as large as 100 μm (Fig. 2a). After pulverisation and 6 h decantation (i.e. the powders after 6 h of decantation), particle sizes were less than 2 μm, with most particles being smaller than 1 μm (Fig. 2b). After pulverisation and 24 h decantation (i.e. the powders after 24 h of decantation), particle sizes were less than 500 nm, with most particles being smaller than 300 nm (Fig. 2c).

3.2 Agglomeration of the powders and a drying technique

After sublimation of the frozen suspension of the powders after 24 h of decantation without CAS conditions, all particles had agglomerated, and no dispersed powder was observed (Fig. 3a). It is likely that the growth of large ice crystals together with the volume change of water during freezing results in the exclusion of powder from the frozen ice and agglomeration of the powder.

After the sublimation of ice (freeze-drying of the powders) in frozen suspension under CAS conditions, a considerable amount of dispersed powder was observed among the agglomerated secondary particles (Fig. 3b), which suggests that CAS freezing is an effective way of obtaining dispersed powders. In frozen suspension under CAS conditions, ice crystals a few tens of micrometres in size are regularly arranged (Fig. 3c), suggesting that ice caused the agglomeration of powders.

After sublimation of the ice in a frozen suspension with ethanol as a dissolved solvent under CAS conditions, most of the powders are dispersed, although agglomerated secondary particles remained (Fig. 3d). Figure 2d indicates an example of secondary particles observed under an SEM after sublimation of a frozen suspension with ethanol as a dissolved solvent. The size of the secondary particle is about a few tens of micrometres, and the secondary particle is agglomeration of fine-grained particles less than a few hundred nanometres in size. Our observations indicate that the powders prepared by freeze-drying of a frozen suspension with ethanol as the dissolved solvent under CAS conditions are adequately

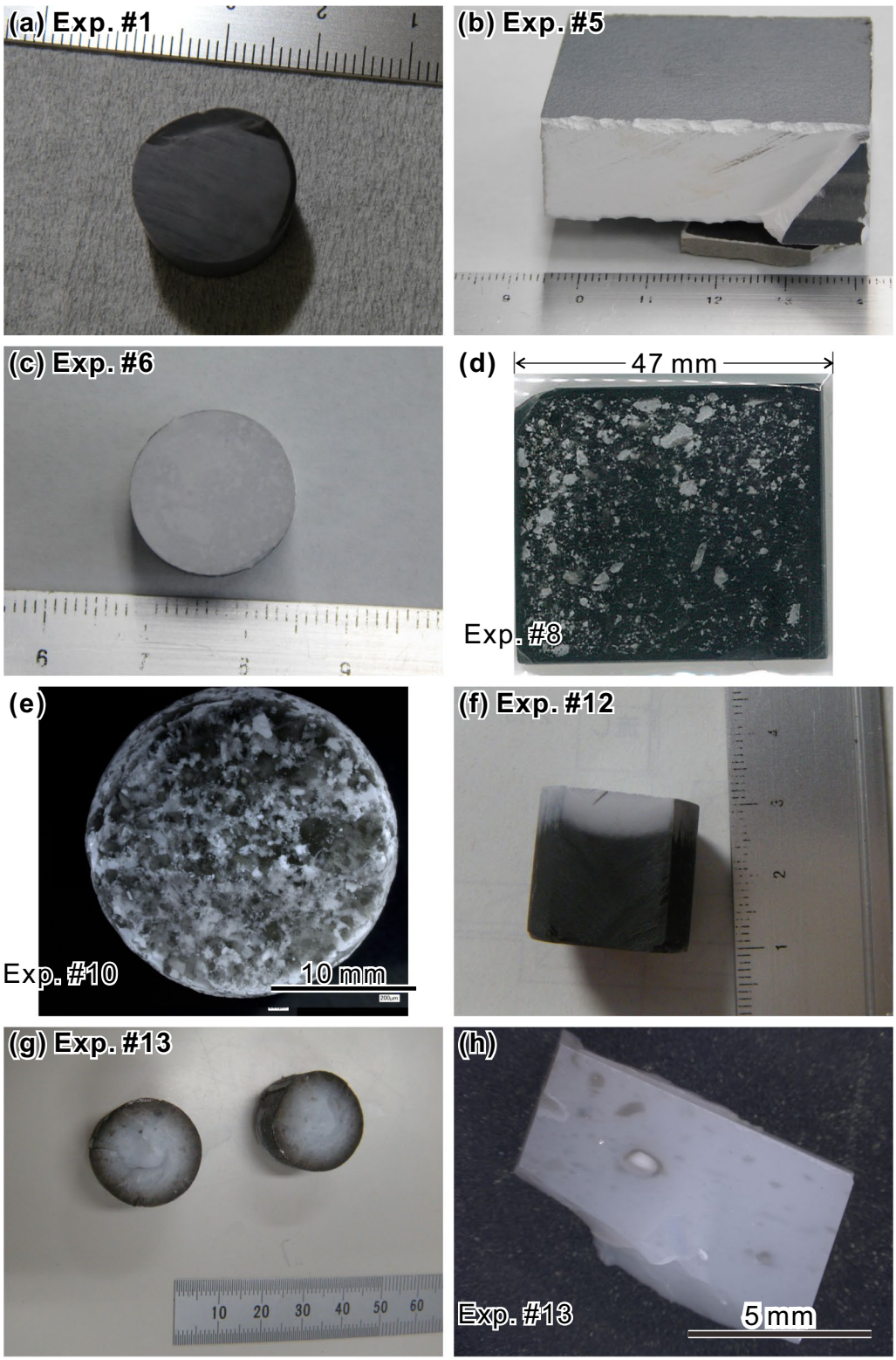

Fig. 4 Visual appearance of hot-pressed samples. **a**, **b** Samples from the powders after 6 h of decantation and hot-pressed at 50 MPa and **a** 1150 °C (Exp. #1) and **b** 1050 °C (Exp. #5). **c**, **d** Samples from the powders after 24 h of decantation and hot-pressed without CAS conditions at 50 MPa and 1100 °C for **c** 17 h (Exp. #6) and **d** 100 h (Exp. #8). **e**, **f** Sample from the powders after 24 h of decantation and hot-pressed **e** without (Exp. #10) and **f** with (Exp. #12) CAS conditions at 1080 °C and 100 MPa. **g**, **h** Sample prepared from a green body by slip casting and hot-pressed at 1080 °C and 120 MPa (Exp. #13)

Table 2 Summary of the results of hot pressing

Exp. No.	Weight (g)	Shape	Bottom area (mm^2)	Height (mm)	Volume (cm^3)	Apparent density ($\times 10^3$ kg m^{-3})	Apparent porosity (%)	Visual appearance	Partial melt?
#1	6.97	Cylinder	186.27	14.50	2.70	2.58	1.5	Black	P. melt
#2	7.55	Cylinder	188.69	15.70	2.96	2.55	2.7	Black and white mottled	P. melt
#3	7.90	Cylinder	205.10	21.50	4.41	1.79	31.6	White	–
#4	7.74	Cylinder	202.07	25.94	5.24	1.48	43.6	White	–
#5	59.27	Rectangular	1974.00	18.00	35.53	1.67	36.3	White	–
#6	7.02	Cylinder	204.85	16.08	3.29	2.13	18.7	Grey and white mottled	P. melt
#7	7.13	Cylinder	203.58	14.10	2.87	2.48	5.2	Black and white mottled	P. melt
#8	32.018	Rectangular	1974.00	6.20	12.24	2.62	0.1	Black (white mottled)	P. melt
#9	18.50	Cylinder	339.79	24.50	8.32	2.22	15.2	Grey and white mottled	–
#10	20.675	Cylinder	339.79	24.00	8.16	2.54	3.2	Black and white mottled	–
#11	17.89	Cylinder	356.33	21.75	7.75	2.31	11.9	Black (partly-white)	–
#12	16.60	Cylinder	346.36	19.20	6.65	2.50	4.7	Black (partly white)	–
#13	23.56	Cylinder	350.66	25.67	9.00	2.62	0.1	White	–
#14	19.79	Rectangular	780.30	10.70	8.35	2.37	9.5	White	–
#15	22.55	Rectangular	779.28	11.55	9.00	2.51	4.4	White	–
#16	29.80	Rectangular	785.40	14.50	11.39	2.62	0.1	Black	–
#17	27.76	Rectangular	785.40	13.50	10.60	2.62	0.1	Greenish grey	–
#18	30.01	Rectangular	785.40	14.59	11.46	2.62	0.04	White	–

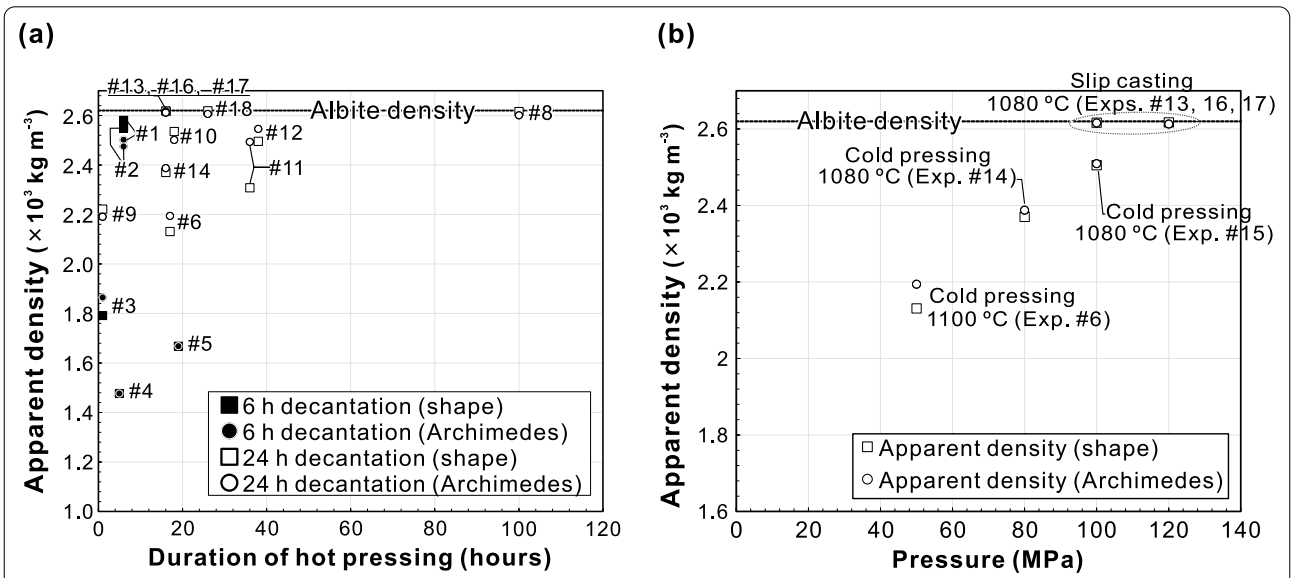

Fig. 5 Apparent density of the samples after hot pressing. Data are also shown in Tables 1, 3. **a** Relationship between the apparent density and duration of hot pressing. The experimental numbers are annotated on the figure. See Table 1 for the experimental conditions. **b** Relationship between the apparent density and pressure. The experimental numbers, temperatures and forming methods are annotated on the figure

Table 3 Evaluation of densification using Archimedes' principle

Exp. No.	Archimedes' method						Shape measurement	
	Weight (g)	Buoyancy force (gw)	Standard deviation (gw)	Volume (cm^3)	Apparent density ($\times 10^3$ kg m^{-3})	Apparent porosity (%)	Apparent density ($\times 10^3$ kg m^{-3})	Apparent porosity (%)
#1	6.52	2.60	0.01	2.61	2.50	4.52	2.58	1.50
#2	7.10	2.86	0.01	2.87	2.48	5.53	2.55	2.73
#3	7.10	3.80	0.01	3.81	1.87	28.81	1.79	31.62
#4	–	–	–	–	–	–	1.48	43.64
#5	–	–	–	–	–	–	1.67	36.33
#6	6.77	3.08	0.01	3.09	2.19	16.26	2.13	18.66
#7	6.79	2.66	0.00	2.67	2.54	2.87	2.48	5.20
#8	23.71	9.10	0.01	9.12	2.60	0.74	2.62	0.15
#9	17.92	8.16	0.03	8.18	2.19	16.37	2.22	15.18
#10	20.68	8.25	0.02	8.27	2.50	4.54	2.54	3.24
#11	18.12	7.26	0.01	7.27	2.49	4.84	2.31	11.89
#12	15.12	5.93	0.01	5.94	2.55	2.83	2.50	4.74
#13	2.43	0.93	0.01	0.93	2.61	0.27	2.62	0.10
#14	19.51	8.16	0.01	8.17	2.39	8.87	2.37	9.53
#15	11.12	4.42	0.03	4.43	2.51	4.22	2.51	4.38
#16	14.78	5.64	0.01	5.65	2.62	0.16	2.62	0.13
#17	14.27	5.45	0.02	5.46	2.61	0.32	2.62	0.07
#18	1.04	0.40	0.01	0.40	2.61	0.53	2.62	0.04

dispersed. In the rest of this paper, our reference to the powders after 24 h of decantation with CAS conditions indicates that the powder was prepared by freeze-drying of a frozen suspension under CAS conditions with ethanol as the dissolved solvent.

3.3 Sintering by hot pressing

3.3.1 Experiments using the powders after 6 h of decantation

The sample that was hot-pressed at a temperature of 1150 °C and a pressure of 50 MPa for 6 h (Exp. #1) has a black colour appearance (Fig. 4a), and the weight and volume are 6.97×10^{-3} kg and 2.70×10^{-6} m^3, respectively (Table 2; Fig. 5a). Thus, the apparent density obtained through the shape measurement is 2.58×10^3 kg m^{-3}, which is close to the known density of albite (2.62×10^3 kg m^{-3}; Deer et al. 1992). The apparent density obtained by Archimedes' principle is 2.5×10^3 kg m^{-3} (Table 3; Fig. 5a). The reason for the black colour is described later. The density of the sample that was hot-pressed at a temperature of 1125 °C with a pressure of 50 MPa for 6 h (Exp. #2) was estimated through the shape measurement and Archimedes' principle to be 2.55×10^3 kg m^{-3} (Table 2) and 2.48×10^3 kg m^{-3} (Table 3), respectively (Fig. 5a), which is also close to the known density of albite, and this sample has a mottled black and white appearance. The cause of this mottled appearance is described later.

A backscattered electron image (BEI) under the SEM of the mirror-polished surfaces of the sample at 1150 °C and 50 MPa (Exp. #1) indicate that albite particles are surrounded by a melt phase (Fig. 6a). Melt phases are characterised by a darker colour than the albite crystals in these images, and they are commonly observed in intergranular regions of the powder particles in samples that were hot-pressed at temperatures higher than 1100 °C. The amount of melt is smaller in the sample at 1125 °C (Fig. 6b; Exp. 2). Although the samples had almost completely shrunk and had low porosities at temperatures higher than 1100 °C, the shrinkage behaviour observed in the experiments was caused by melting and not solid-state sintering of the powders.

In contrast, the samples that were hot-pressed below 1100 °C (Exps. #3, #4 and #5) show apparent densities less than 2.0×10^3 kg m^{-3} (Tables 2 and 3; Fig. 5a) and are white in appearance (Fig. 4b). The shrinkage behaviour at a temperature of 1050 °C and pressure of 50 MPa (Exp. #5) indicates that the sample started to shrink at ~ 980 °C and that rapid shrinkage occurred as the temperature was increased (Fig. 7a). Gradual shrinking then took place until the end of the experiment, with the rate of shrinkage gradually slowing. These observations indicate the operation of sintering during the hot pressing.

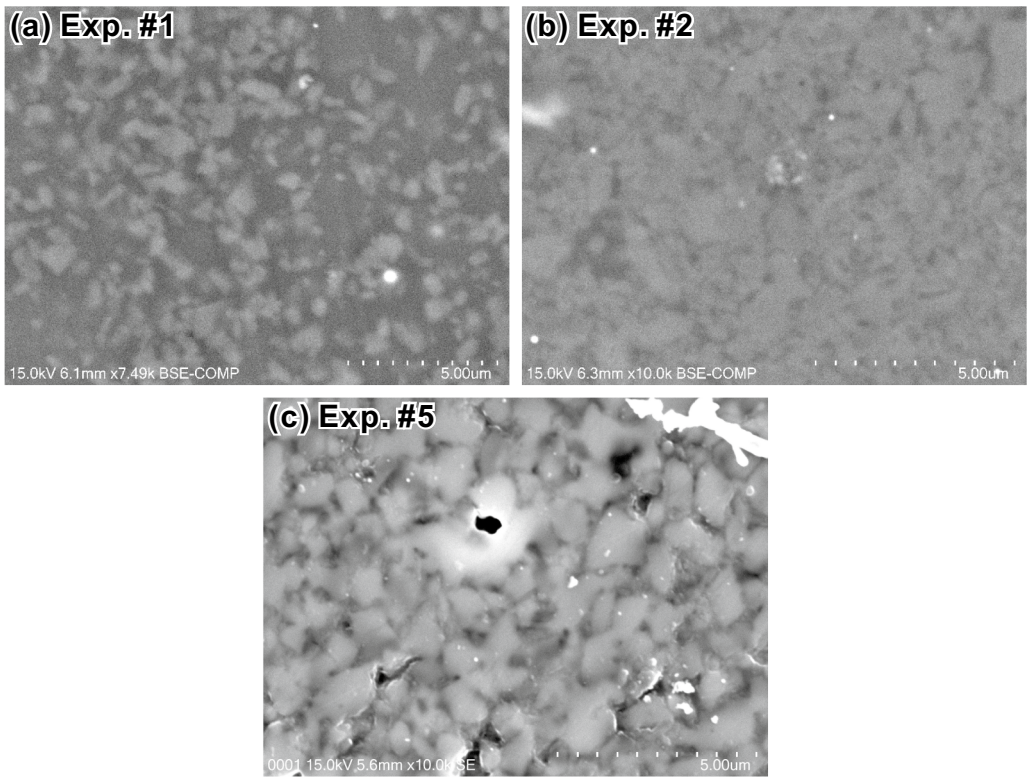

Fig. 6 SEM images of hot-pressed samples prepared from the powders after 6 h of decantation. **a** Backscattered electron image (BEI) of the sample that was hot-pressed at 50 MPa and 1150 °C (Exp. #1). **b** BEI of the sample that was hot-pressed at 50 MPa and 1125 °C (Exp. #2). **c** Secondary electron image (SEI) of the sample that was hot-pressed at 50 MPa and 1050 °C (Exp. #5)

A secondary electron image (SEI) under the SEM indicates that many pores are observed in the samples hot-pressed below 1100 °C using the powders after 6 h of decantation (Fig. 6c; Exps #3, #4 and #5), indicating that the samples were not well sintered. At temperatures lower than 1100 °C, the samples did not shrink entirely and had higher porosities. It is difficult to significantly sinter the powders after 6 h of decantation without melting.

3.3.2 Experiments using the powders after 24 h of decantation without CAS conditions

The sample using the powders after 24 h of decantation without CAS conditions that was hot-pressed at a temperature of 1100 °C and a pressure of 50 MPa for 17 h (Exp. #6) is white in appearance but has a mottled pattern on the surface (Fig. 4c). The apparent densities obtained through shape measurement and Archimedes' principle are 2.13×10^3 and 2.19×10^3 kg m^{-3}, which is much denser than the samples in the experiments using the powders after 6 h of decantation below 1100 °C (Exps. #3 and 6 in Tables 2 and 3; Fig. 5a), and this suggests that the use of fine-grained powders gives rise to the possibility of fabrication. We also subjected this powder to hot pressing under the same temperature and pressure conditions for 100 h (Exp. #8), and this sample was black in appearance with white mottling (Fig. 4d). The apparent densities obtained through shape measurement and Archimedes' principle are 2.62×10^3 kg m^{-3} and 2.60×10^3 kg m^{-3}, which is similar to the known density of albite, indicating dense sintering (Exp. #8 in Tables 2 and 3; Fig. 5a).

The shrinkage behaviour in experiments using the powders after 24 h of decantation at a temperature of 1100 °C and pressure of 50 MPa for 100 h (Fig. 7b, Exp. #8) is similar to that observed for the 6-h powder fraction (Fig. 7a). The sample started to shrink at about 980 °C, and rapid shrinkage occurred when the temperature was increased (Fig. 7b). The samples then shrank gradually until the end of the experiment, with the rate of shrinkage gradually slowing. After almost 80 h, the shrinkage virtually stopped.

Many pores were observed in the sample that was hot-pressed for 17 h (Exp. #6) in an SEI under the SEM (Fig. 8a). In the sample that was hot-pressed for 100 h (Exp. #8), very few pores were observed in most parts of the sample (Fig. 8b, c), but pores are present in the areas

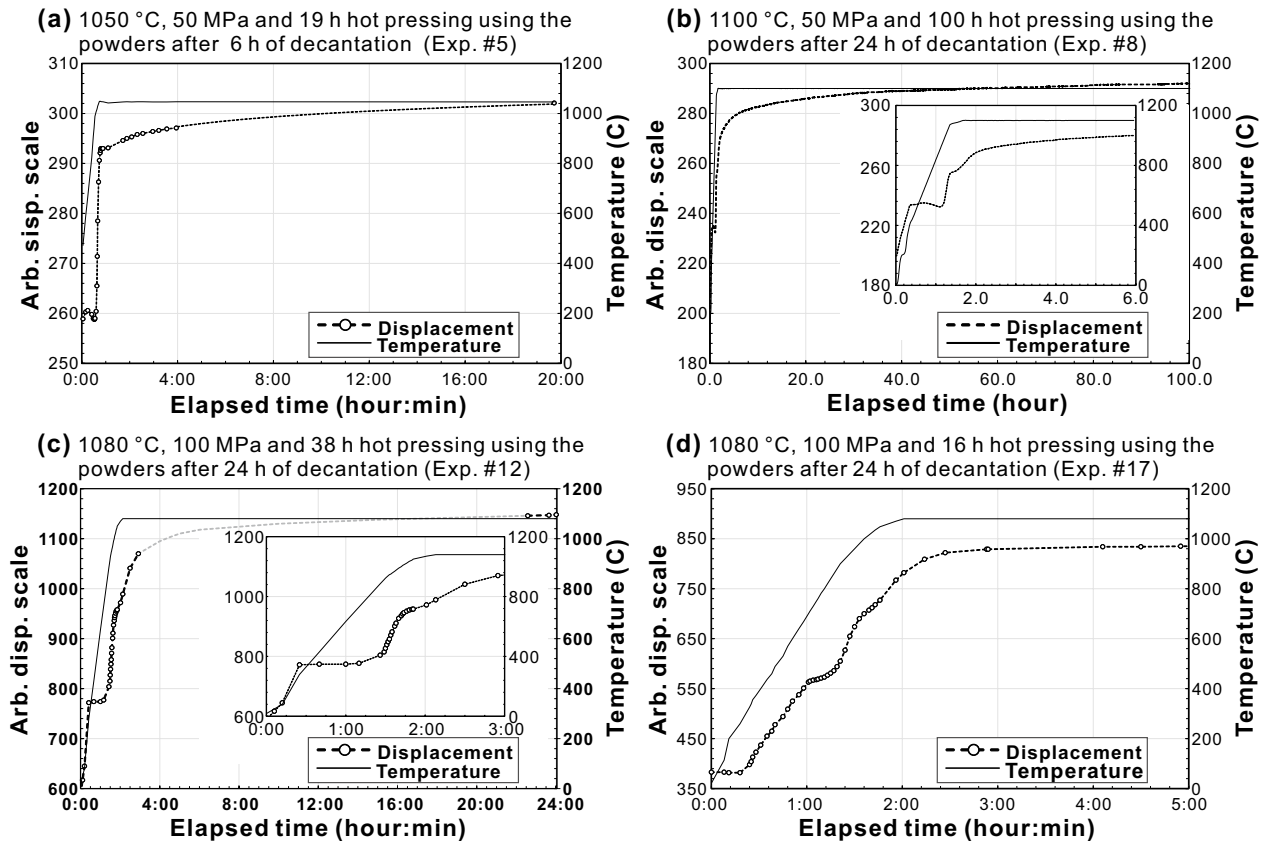

Fig. 7 Shrinkage behaviour during hot pressing. **a** Shrinkage behaviour of the powders after 6 h of decantation and hot-pressed at 50 MPa and 1050 °C (Exp. #5). **b** Shrinkage behaviour of the powders after 24 h of decantation and hot-pressed without CAS conditions at 50 MPa and 1100 °C (Exp. #8). Inset indicates the shrinkage behaviour for the first 6 h. **c** Shrinkage behaviour of the powders after 24 h of decantation and hot-pressed with CAS conditions at 100 MPa and 1080 °C (Exp. #12). Inset indicates the shrinkage behaviour for the first 3 h. **d** Shrinkage behaviour in the experiment of preparing a green body by slip casting from the powders after 24 h of decantation and hot pressing with CAS conditions at 100 MPa and 1080 °C (Exp. #17). The shrinkage behaviour was manually recorded for the experiments shown in (**a**), (**c**) and (**d**), and the open circles indicate the recorded displacements

with white mottling (Fig. 8d, e). The hot pressing time of 17 h was too short to allow for dense sintering, which is consistent with the results of apparent density measurements (Tables 2 and 3; Fig. 5a) and the shrinkage behaviour (Fig. 7b), as mentioned above. However, many darker coloured spots can be seen in the BEI of this sample (Exp. #8), which suggests the presence of a melt phase (Fig. 8c, e). Our results indicate that a long hot pressing time is necessary to fabricate a dense albite aggregate, although it is possible using the powders after 24 h of decantation. The temperature of 1100 °C is too high for solid-state sintering without melting; therefore, we examined the hot pressing at a pressure of 100 MPa and the temperature of 1080 °C.

The sample that was hot-pressed at 1080 °C and 100 MPa for 18 h shows a black and white mottled appearance (Fig. 4e, Exp. #10). The apparent densities obtained by the shape measurement and Archimedes' principle are 2.54×10^3 and 2.50×10^3 kg m^{-3}, which is close to the known density of albite (Exp. #10 in Tables 2 and 3; Fig. 5a). This means that a shorter period of hot pressing achieved densification when compared with the experiments under a pressure of 50 MPa (e.g. Exp. #6). Our experiments clearly indicate that there is a pressure effect, which will be discussed later (Fig. 5b). An SEI under the SEM of the sample is shown in Fig. 7f. The left side of the image corresponds to the mottled white area, and the right side to the mottled black area. Many pores can be observed on the left side of the image, whereas very few pores appear on the right; this indicates that sintering occurred heterogeneously. The mottled black and white areas correspond to densely and poorly sintered parts, respectively. The X-ray spectra obtained for the mottled black and white areas by SEM–EDS do not show any significant difference (Fig. 9a). We suggest

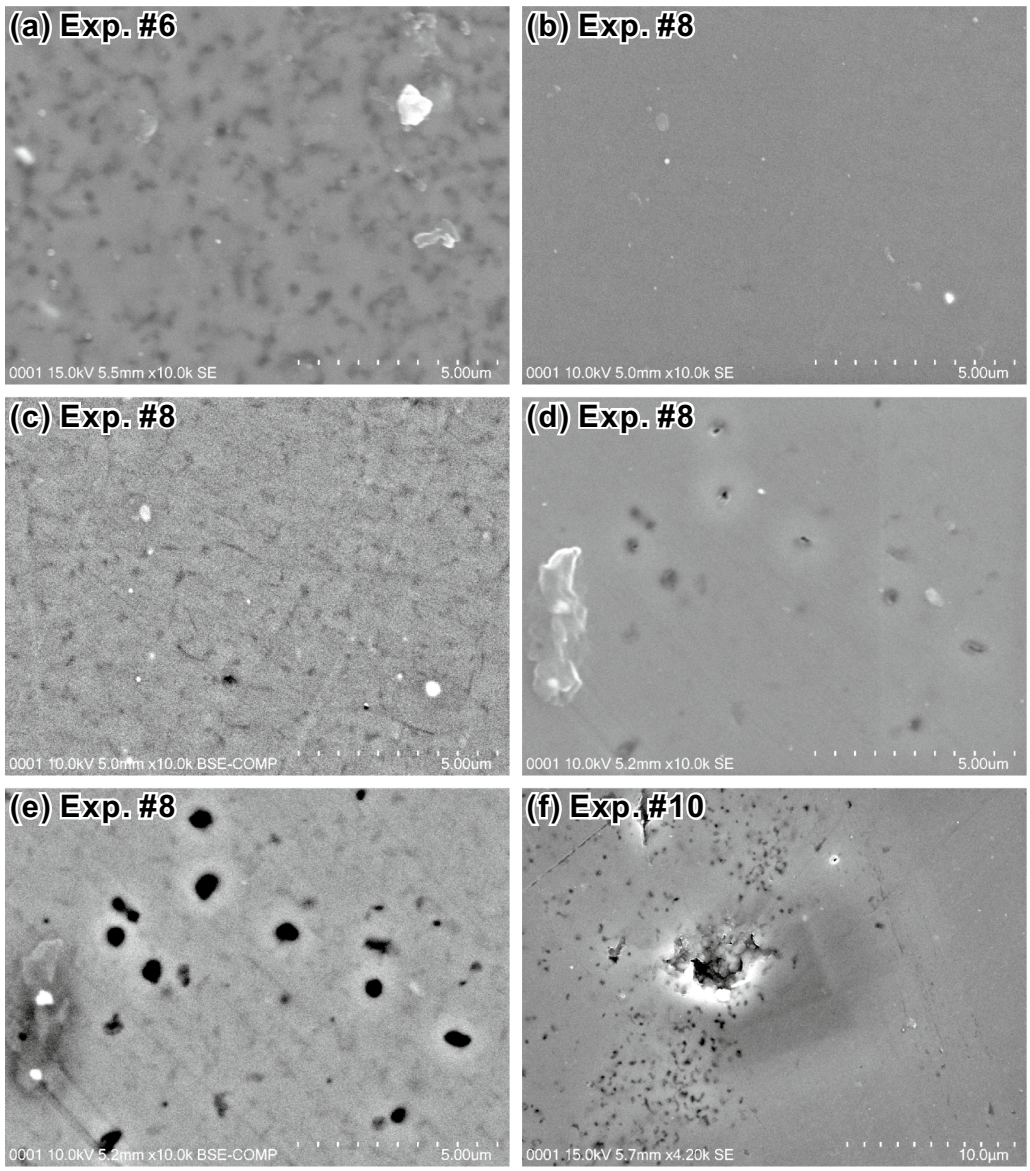

Fig. 8 SEM images of hot-pressed samples prepared from the powders after hours of decantation without CAS conditions. **a** SEI of the sample that was hot-pressed for 17 h at 1100 °C and 50 MPa (Exp. #6). **b** SEI of the sample that was hot-pressed for 100 h at 1100 °C and 50 MPa (Exp. #8). **c** BEI of the same place as (**b**). **d** SEI of the sample that was hot-pressed for 100 h at 1100 °C and 50 MPa and was mottled white (Exp. #8). **e** BEI of the same place as (**d**). **f** SEI of the sample that was hot-pressed for 18 h at 1080 °C and 100 MPa (Exp. #10). The left side of the image corresponds to the white mottled area, and the right side of the image corresponds to the black mottled area

that the larger agglomerates of secondary particles sintered more quickly than the surrounding powder and that the sintered secondary grains support each other, thus preventing further sintering of the powder between the sintered secondary grains and resulting in the heterogeneous sintering.

3.3.3 Experiments using the powders after 24 h of decantation with CAS conditions

The samples that were hot-pressed using the powders after 24 h of decantation with CAS conditions at a pressure of 100 MPa (Exps. #11 and #12) have a black bottom part and an upper white part (Fig. 4f). Figure 10a shows

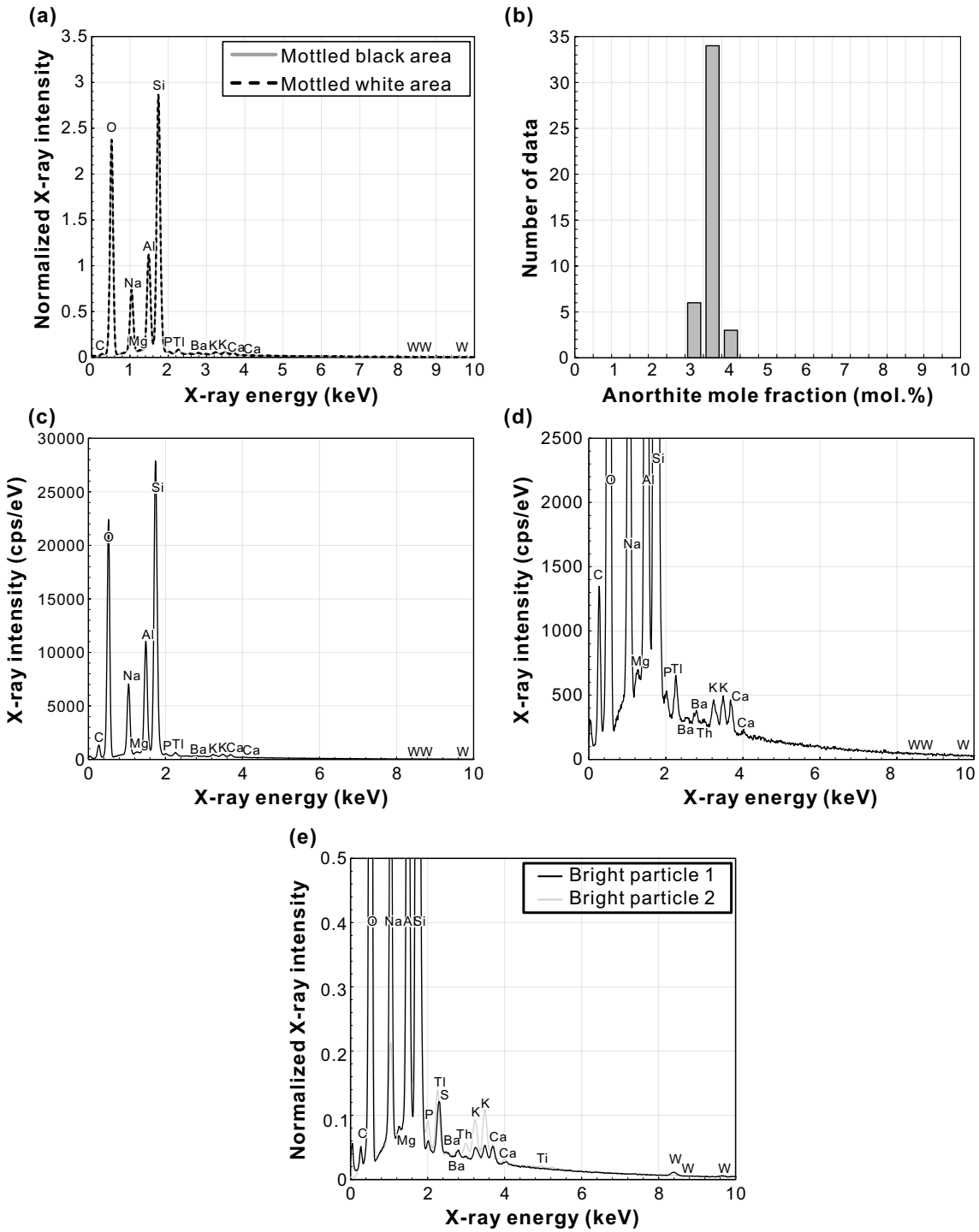

Fig. 9 Chemical analyses of hot-pressed samples. **a** X-ray spectra of the mottled black (grey solid line) and white (black solid line) areas (Exp. #10). The X-ray intensity is normalised by the total X-ray intensity from 0 to 20 keV. **b** Anorthite mole fraction for a dense albite aggregate (Exp. #13). **c** X-ray spectrum of a dense albite aggregate (Exp. #13; SEM–EDS). **d** The same X-ray spectrum in (**c**), but with a normalised X-ray intensity of < 0.3. **e** X-ray spectra of the bright particles observed in SEM images. The X-ray intensity is normalised by the total X-ray intensity from 0 to 20 keV. Bright particles 1 and 2 were in the samples from Exp. #10 and #13, respectively

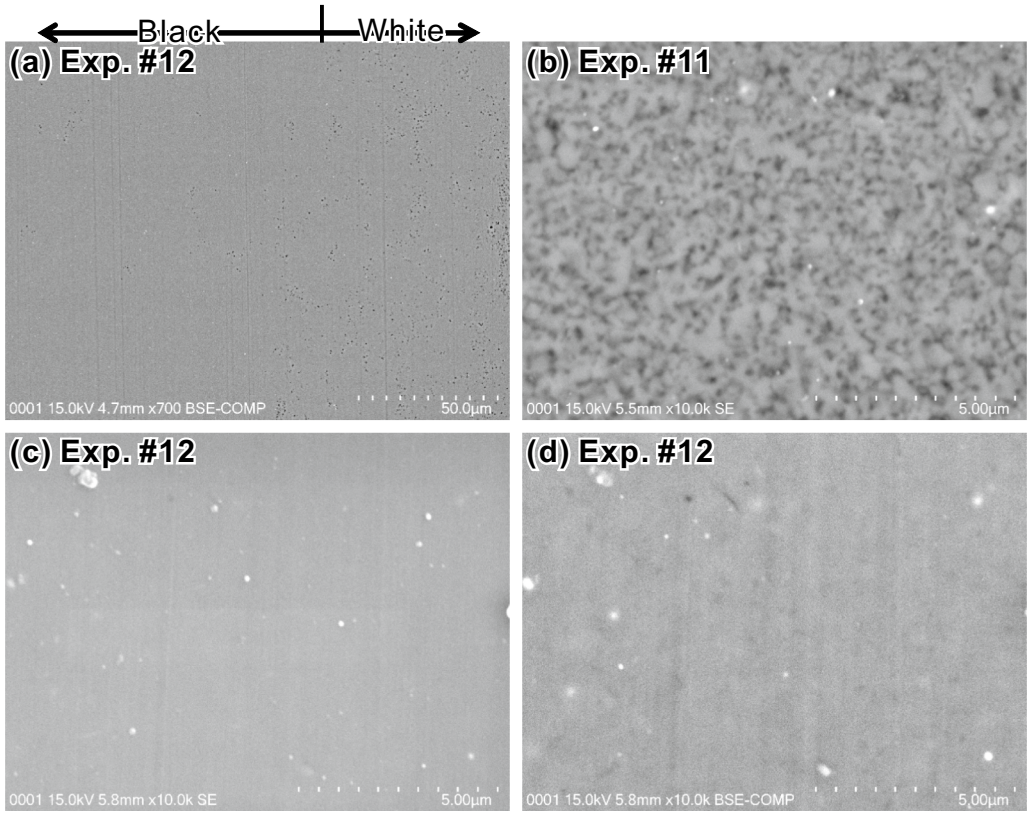

Fig. 10 SEM images of samples prepared from the powders after 24 h of decantation that were hot-pressed with CAS conditions at 1080 °C and 100 MPa for 36 (Exp. #11) or 38 (Exp. #12) hours. **a** SEI of the boundary region between black (left) and white (right) coloured parts (see Fig. 4f). **b** SEI of the white coloured part of the sample. **c** SEI of the black coloured part of the sample. **d** BEI of the same place as (**c**)

a BEI under the SEM of the boundary region between the white (right side of Fig. 10a) and black (left side of Fig. 10a) parts. White parts contain many pores (Fig. 10a, b), whereas the black parts contain very few (Fig. 10a, c). The black part of the samples is well sintered. Although the apparent densities of the samples (2.31×10^3 kg m^{-3} (shape) and 2.49×10^3 kg m^{-3} (Archimedes) for Exp. #11 and 2.50×10^3 kg m^{-3} (shape) and 2.55×10^3 kg m^{-3} (Archimedes) are lower than the known density of albite, the values are averages of densely and poorly sintered parts (Tables 2 and 3; Fig. 5a). In the BEI under the SEM, very few darker coloured spots can be seen (Fig. 10d), which suggests that the sintering temperature of 1080 °C is below the solidus temperature of albite.

Some experimental results indicate that the apparent density after the hot pressing increases with pressure (Fig. 5b). The durations of hot pressing of the experiments shown in Fig. 5b are 16 or 17 h, and these experiments used the powders after 24 h of decantation. The experimental conditions were similar except for the pressure.

We further examined hot pressing of green bodies prepared by slip casting at the same temperature and under pressures ranging from 100 to 120 MPa (Table 1, Exps. #13, #16, #17 and #18). The apparent densities of all samples prepared from green bodies are $> 2.60 \times 10^3$ kg m^{-3}, which is similar to the known density of albite (Tables 2 and 3; Fig. 5a), indicating dense sintering. Samples dewaxed for more than 5 h (Exps #13 and #18) are white (Fig. 4g, h).

The shrinkage behaviours in experiments using the powders after 24 h of decantation with CAS conditions, both with and without the preparation of green bodies, are shown in Fig. 7c (Exp. #12) and Fig. 7d (Exp. #17), respectively. In both experiments, the sample started to shrink at ~ 800 °C and rapid shrinkage occurred when the temperature was increased (Fig. 7c, d). The samples shrank more gradually when the temperature was kept constant at 1080 °C.

There is a difference in the shrinkage behaviour in the experiments with and without the preparation of green bodies. The samples in the experiments without

Table 4 Example of chemical compositions of a hot-pressed sample (Exp. #13)

Analytical points	1	2	3	4	5	6	7	8	9	10	11
SiO_2 (Oxide wt.%)	69.65	68.98	69.42	69.22	69.48	69.23	69.46	69.34	69.37	69.16	69.35
Al_2O_3 (Oxide wt.%)	20.44	20.45	20.61	20.83	20.61	20.82	20.63	20.69	20.60	20.46	20.61
Na_2O (Oxide wt.%)	11.65	11.50	11.67	11.62	11.63	11.65	11.60	11.53	11.60	11.47	11.69
K_2O (Oxide wt.%)	0.03	0.00	0.00	0.00	0.00	0.00	0.01	0.00	0.00	0.00	0.04
CaO (Oxide wt.%)	0.84	0.76	0.79	0.79	0.78	0.77	0.17	0.75	0.77	0.82	0.78
MgO (Oxide wt.%)	0.02	0.19	0.18	0.21	0.17	0.25	0.17	0.17	0.13	0.17	0.17
BaO (Oxide wt.%)	0.00	0.00	0.11	0.04	0.00	0.00	0.08	0.11	0.00	0.00	0.00
P_2O_5 (Oxide wt.%)	0.30	0.39	0.36	0.36	0.37	0.40	0.27	0.34	0.39	0.39	0.43
Tl_2O (Oxide wt.%)	0.73	0.63	0.75	0.68	0.74	0.59	0.02	0.76	0.69	0.65	0.68
Total (Oxide wt.%)	103.66	102.90	103.89	103.75	103.78	103.71	102.41	103.69	103.55	103.12	103.75
Si (No. of cations)	2.95	2.95	2.95	2.94	2.95	2.94	2.95	2.95	2.95	2.95	2.94
Al (No. of cations)	1.02	1.03	1.03	1.04	1.03	1.04	1.03	1.04	1.03	1.03	1.03
Na (No. of cations)	0.96	0.95	0.96	0.96	0.96	0.96	0.96	0.95	0.96	0.95	0.96
K (No. of cations)	0.00	0.00	0.00	0.00	0.00	0.00	0.00	0.00	0.00	0.00	0.00
Ca (No. of cations)	0.04	0.04	0.04	0.04	0.04	0.04	0.04	0.04	0.04	0.04	0.04
Mg (No. of cations)	0.01	0.01	0.01	0.02	0.01	0.02	0.01	0.01	0.02	0.01	0.01
Ba (No. of cations)	0.00	0.00	0.00	0.00	0.00	0.00	0.00	0.00	0.00	0.00	0.00
P (No. of cations)	0.01	0.02	0.02	0.02	0.02	0.02	0.01	0.01	0.02	0.02	0.02
Tl (No. of cations)	0.01	0.01	0.01	0.01	0.01	0.01	0.01	0.01	0.01	0.01	0.01
An (mol%)	4.02	3.55	3.52	3.54	3.54	3.54	3.54	3.55	3.54	4.06	3.52
Ab (mol%)	95.98	96.45	96.48	96.46	96.46	96.46	96.46	96.45	96.46	95.94	96.48

the preparation of green bodies shrank until the end of each experiment, and the shrinkage continued for more than 3 h after the start of each experiment (Fig. 7c). In contrast, the shrinkage almost stopped after 3 h after the start of each experiment with the preparation of green bodies (Fig. 7d), indicating that the samples were well sintered within a few hours. Sintering occurred more effectively in the experiments with the preparation of green bodies by slip casting. Because fine-grained albite powders agglomerate more easily, as mentioned above, we suggest that the preparation of green bodies by slip casting strengthens the cohesion among particles before hot pressing, thus making it easier to sinter the particles.

The colour of the dense albite aggregates fabricated in this study (Exps. #11, #12, #13, #16, #17 and #18) depends on the duration of dewaxing (Table 2; Fig. 4). The colours of the samples without dewaxing are black (Exps. #11, #12, and #16; Table 2; Fig. 4f), while those after dewaxing for > 5 h are white (Exps. 13 and 18; Table 2; Fig. 4h). This indicates that the albite powders contain organic matter, and the black colour of some samples is due to the presence of carbon, because dewaxing removes organic matter from the samples.

3.4 Features of the dense albite aggregates

During our experiments, we succeeded in obtaining dense albite aggregate (Exps. #11, #12, #13, #16, #17 and #18). An X-ray diffraction (XRD) pattern for a dense albite aggregate (Exp. #13) is shown in Fig. 1b. Most of the peaks could be indexed as either low or high albite. However, although high albite cannot account for some peaks such as those at 33.77° ($\bar{1}32$) and 35.18° ($24\bar{1}$), other peaks are very close to those of high albite, such as peaks at 15.15° ($11\bar{1}$) and 23.77° ($1\bar{3}0$). Thus, some of low albite seems to have been transformed to high albite during the hot pressing. The results of chemical analysis of a dense albite aggregate (Exp. #13) are shown in Fig. 9b–d and Table 4. The anorthite mole fraction of the albite aggregate ranges from 3 to 4 mol% (Fig. 9b; Table 4), and O, Si, Al, Na, K and Ca were detected as major elements and Mg, P, Tl and Ba were detected as minor elements (Fig. 9c; Table 4). The X-ray spectrum for the dense albite aggregate does not show the presence of W, suggesting that the chemical composition was not affected by contamination during pulverisation. However, the X-ray spectra (Fig. 9e) obtained for bright particles in BEIs (e.g. Figs. 8c and 10d) identified two types of bright particles.

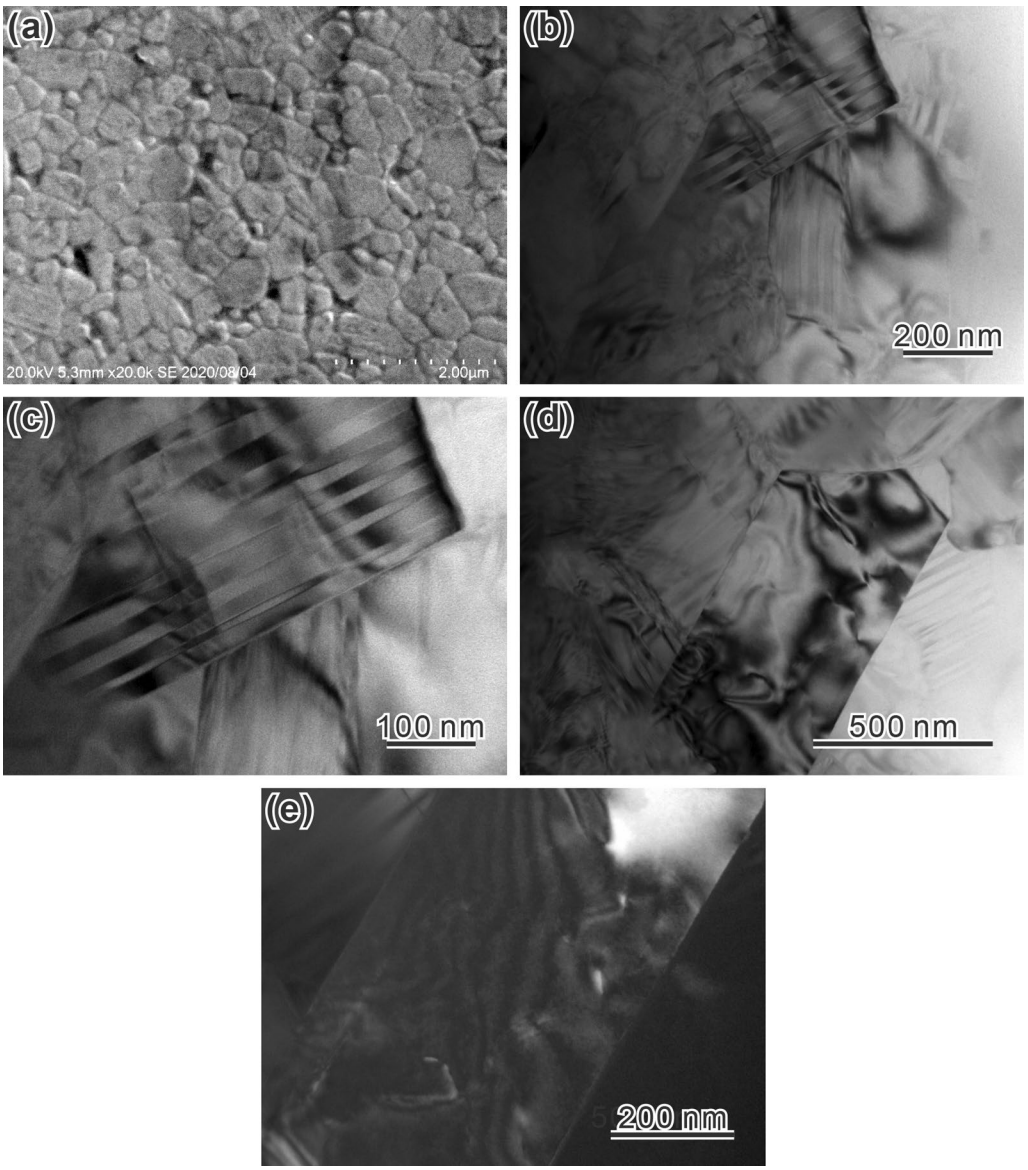

Fig. 11 Microstructural features of the dense albite aggregates. **a** SEI of a dense albite aggregate (Exp. #13) after 51 h annealing at 1050 °C. **b**–**d** TEM bright-field (BF) images of a dense albite aggregate (Exp. #12). **c** An enlarged image of (**b**). **e** TEM dark-field (DF) image of a dense albite aggregate (Exp. #12). The grain in (**e**) is the same as that in (**d**) under different diffraction conditions

One contains W suggesting that the particles represent contamination during pulverisation (bright particle 1 in Fig. 9e). The other does not contain W, but contains Th, suggesting that the particles represent some minerals that were contained in the raw powder (bright particle 2 in Fig. 9e).

Figure 11a shows the microstructure of a dense albite aggregate (Exp. #13) after 51 h of annealing at 1050 °C in the atmosphere, with grain boundaries that were thermally etched. The microstructure is homogeneous and consists of fine grains less than a few hundred nanometres in size, which is similar to the particle size of the starting powder (Fig. 2c). The grain boundaries in the dense albite aggregate (Exp. #12) are not open, and a melt phase is not present along the boundaries (TEM images, Fig. 11b, c), which indicates that the sample was well sintered without melting and that the hot pressing temperature of 1080 °C is below the solidus temperature of albite. Many grains contain fine-scale polysynthetic twins just a few tens of nanometres thick (Fig. 11b–d). Although albite and pericline twins are commonly present as polysynthetic twins in

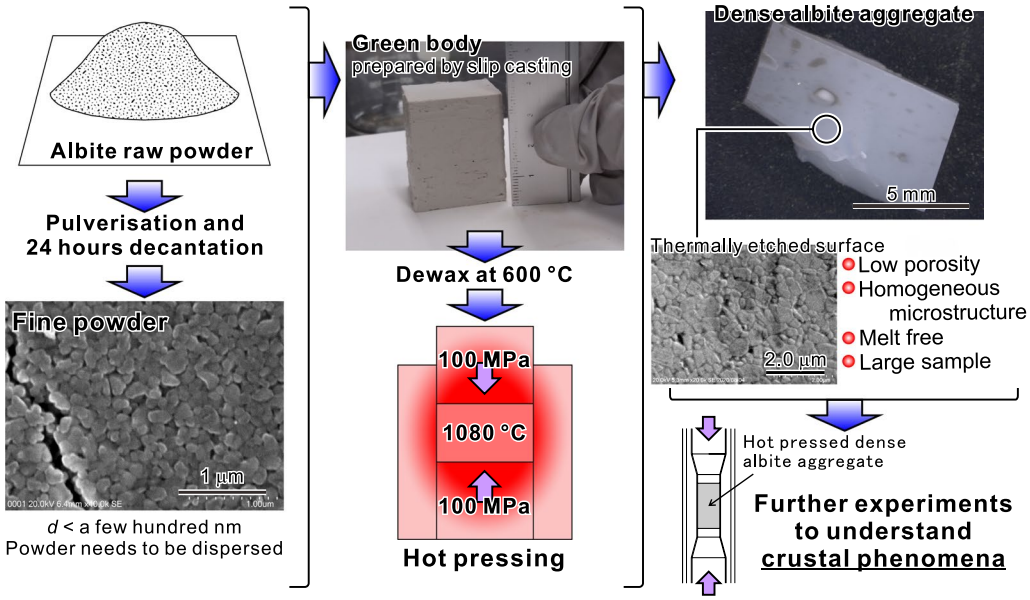

Fig. 12 Workflow to obtain dense albite aggregates

plagioclase, we did not determine the twin law for the twins in our samples. The observed grains sometimes contain considerable amount of dislocations (Fig. 11d, e). These dislocations were possibly formed by differential stress during hot pressing. We still need to improve our technique in order to prepare dense albite aggregate without dislocations.

The workflow to obtain dense albite aggregates is shown in Fig. 12. Fine-grained powders with a particle size less than a few hundred nanometres need to be prepared. These powders should be adequately dispersed. Then, a green body is prepared from the slurry of fine powder using the technique of slip casting. After dewaxing, the green body is hot-pressed in a vacuum at a temperature of 1080 °C and a pressure of 100 MPa, and a dense albite aggregate is obtained. The albite aggregates produced have low porosities, homogeneous microstructures, the absence of melt and sample sizes larger than a cubic centimetre.

The grain size of the albite in the aggregates we produced is very fine, about a few hundred nanometres. This grain size is close to that of feldspar in ultramylonites in shear zones in the crust (e.g. Shigematsu 1999). The aggregates we produced can, therefore, be used as analogues of the shear zones that are often developed as deep extensions of seismogenically active faults (e.g. Norris and Cooper 2007). However, coarse-grained rocks also exist in the Earth's crust. Thus, preparing coarse-grained aggregates of Na-rich plagioclase is one of the next challenges we should face. We hope that the albite aggregates prepared by this technique provide new opportunities for conducting experiments that help us to understand crustal phenomena.

4 Conclusions

We explored a method of fabricating dense aggregates of albite by hot pressing. During our experiments, the particle size of the powdered albite, the agglomeration of the powders, the method of forming, the sintering temperature, and the pressure and duration of the hot pressing were varied. We found that the following factors are important when fabricating a dense aggregate of albite.

1. The particle size of the powder needs to be less than a few hundred nanometres. We prepared the powder by pulverisation of natural albite and decantation.
2. The powder needs to be adequately dispersed. We developed a technique of dispersing the powder during freeze-drying.
3. Preparation of a green body by slip casting makes the process of hot pressing efficient.

Then, it is possible to obtain a dense aggregate of albite by hot pressing at a temperature of 1080 °C and a pressure of 100 MPa. The albite aggregates produced have low porosities, homogeneous microstructures, the absence of melt and sample sizes larger than a cubic centimetre. We hope that the albite aggregates prepared by this technique provide new opportunities for conducting experiments that help us to understand crustal phenomena.

Abbreviations
XRD: X-ray diffraction; SEM: Scanning electron microscope; CAS: Cell alive system; TEM: Transmission electron microscope; EDS: Energy-dispersive spectroscope; BEI: Backscattered electron image; SEI: Secondary electron image; GSJ: Geological Survey of Japan; AIST: National Institute of Advance Industrial Science and Technology.

Acknowledgements
We thank Takashi Okai, Atsuyuki Ohta and Ran Kubota for the use of a freeze dryer at the IGG of GSJ, AIST. NS and MK have benefited from discussions with Akihiko Tomiya, Takayuki Nakatani and Isoji Miyagi at IEVG of GSJ, AIST. NS and MK have also benefited from discussions with Yuki Tsunazawa and Yoshiaki Kon at GREEN of GSJ about the pulverisation of albite powders. T. Hiraga and an anonymous reviewer provided helpful comments that led to improvements in this manuscript.

Authors' information
MK is now at Sapporo regional headquarters Japan Meteorological Agency. MK was involved in this research when he was at Research Institute of Earthquake and Volcano Geology, Geological Survey of Japan, National Institute of Advanced Industrial Science and Technology.

Author contributions
NS planned this study, and ZY, HH and YY contributed to the details. NS examined methods for preparing dispersed submicron albite powders for sintering, and NS and MK prepared the powders. NS drafted the main part of the paper. All authors contributed to the interpretations of the data and assisted in drafting the paper. All authors read and approved the final manuscript.

Funding
This work was partially supported by a grant from MEXT Kakenhi (No. 26109004).

Availability of data and materials
The data sets used and/or analysed during the current study are available from the corresponding author on reasonable request.

Declarations

Competing interests
The authors declare that they have no competing interest.

Author details
[1]Research Institute of Earthquake and Volcano Geology, Geological Survey of Japan, National Institute of Advanced Industrial Science and Technology, Tsukuba 305-8567, Japan. [2]Multi-Material Research Institute, National Institute of Advanced Industrial Science and Technology, Nagoya 463-8560, Japan. [3]Sapporo Regional Headquarters Japan Meteorological Agency, Sapporo 060-0002, Japan.

Received: 2 December 2021 Accepted: 20 May 2022
Published online: 11 June 2022

References
Carpenter MA (1991) Mechanisms and kinetics of Al–Si ordering in anorthite: I. Incommensurate structure and domain coarsening. Am Mineral 76:1110–1119
Deer WA, Howie RA, Zussman J (1992) An introduction to rock-forming minerals, 2nd edn. Person Education Limited, Essex
Dresen G, Wang G, Bai Q (1996) Kinetics of grain growth in anorthite. Tectonophysics 258:251–262. https://doi.org/10.1016/0040-1951(95)00203-0
Farver J, Yund RA (1995a) Interphase boundary diffusion of oxygen and potassium in K-feldspar/quartz aggregates. Geochim Cosmochim Acta 59:3697–3705
Farver J, Yund RA (1995b) Grain boundary diffusion of oxygen, potassium and calcium in natural and hot-pressed feldspar aggregate. Contrib Mineral Petrol 118:340–355
Fukuda J, Muto J, Nagahama H (2018) Strain localization and fabric development in polycrystalline anorthite + melt by water diffusion in an axial deformation experiment. Earth Planets Space 70:3. https://doi.org/10.1186/s40623-017-0776-2
Fukushima M, Tsuda S, Yoshizawa Y (2013) Fabrication of highly porous alumina prepared by gelation freezing route. J Am Ceram Soc 96:1029–1031. https://doi.org/10.1111/jace.12229
Hiraga T, Miyazaki T, Tasaka M, Yoshida H (2010) Mantle superplasticity and its self-made demise. Nature 468:1091–1094. https://doi.org/10.1038/nature09685
Kang SJL (2005) Sintering: densification, grain growth and microstructure. Elsevier Butterworth-Heinemann, Oxford
Karato S (2010) Rheology of the deep upper mantle and its implications for the preservation of the continental roots: a review. Tectonophysics 481:82–98. https://doi.org/10.1016/j.tecto.2009.04.011
Koizumi S, Hiraga T, Tachibana C, Tasaka M, Miyazaki T, Kobayashi T, Takamasa A, Ohashi N, Sano S (2010) Synthesis of highly dense and fine-grained aggregates of mantle composites by vacuum sintering of nano-sized mineral powders. Phys Chem Miner 37:505–518. https://doi.org/10.1007/s00269-009-0350-y
Li L, Wang B, Arakawa M (1991) The relationship between the pore characteristics and the suctionability of a gypsum mold. J Soc Powder Technol 28:684–688 (**in Japanese with English abstract**)
Luan FC, Paterson MS (1992) Preparation and deformation of synthetic aggregates of quartz. J Geophys Res Solid Earth 97:301–320
Miyazaki T, Sueyoshi K, Hiraga T (2013) Olivine crystals align during diffusion creep of Earth's upper mantle. Nature 502:321–326. https://doi.org/10.1038/nature12570
Morono Y, Terada T, Yamamoto Y, Xiao N, Hirose T, Sugeno M, Ohwada N, Inagaki F (2015) Intact preservation of environmental samples by freezing under an alternating magnetic field. Environ Microbiol Rep 7:245–251. https://doi.org/10.1111/1758-2229.12238
Norris RJ, Cooper FA (2007) The alpine fault, New Zealand: surface geology and field relationships. In: Okaya D, Stern TA, Davey F (eds) A continental plate boundary: tectonics at South Island, New Zealand. Geophysical monograph series, vol 175, pp 157–175. https://doi.org/10.1029/175GM09
Rybacki E, Dresen G (2000) Dislocation and diffusion creep of synthetic anorthite aggregates. J Geophys Res Solid Earth 105:26017–26036. https://doi.org/10.1029/2000JB900223
Rybacki E, Wirth R, Dresen G (2010) Superplasticity and ductile fracture of synthetic feldspar deformed to large strain. J Geophys Res Solid Earth 115:B08209. https://doi.org/10.1029/2009JB007203
Shigematsu N (1999) Dynamic recrystallization in deformed plagioclase during progressive shear deformation. Tectonophysics 305:437–452. https://doi.org/10.1016/S0040-1951(99)00039-6
Tasaka M, Hiraga T (2013) Influence of mineral fraction on the rheological properties of forsterite + enstatite during grain-size-sensitive creep: 1. Grain size and grain growth laws. J Geophys Res Solid Earth 118:3970–3990. https://doi.org/10.1002/jgrb.50285
Tsubokawa Y, Ishikawa M (2017) Sintering nanocrystalline diopside from pulverized diopside crystals. J Mineral Petrol Sci 112:127–131. https://doi.org/10.2465/jmps.161114c
Tullis J, Yund RA (1985) Dynamic recrystallization of feldspar: a mechanism for ductile shear zone formation. Geology 13:238–241
Yabe K, Sueyoshi K, Hiraga T (2020) Grain-boundary diffusion creep of olivine: 1. Experiments at 1 atm. J Geophys Res Solid Earth 125:e2020JB019415. https://doi.org/10.1029/2020JB019415

Publisher's Note